Article

Stigmatellin Probes the Electrostatic Potential in the Q_B Site of the Photosynthetic Reaction Center

László Gerencsér,[1,5,*] Bogáta Boros,[1] Valerie Derrien,[2] Deborah K. Hanson,[3] Colin A. Wraight,[4] Pierre Sebban,[2] and Péter Maróti[1,*]

[1]Department of Biophysics, University of Szeged, Szeged, Hungary; [2]Laboratoire de Chimie Physique, University of Paris-Sud, Orsay, France; [3]Biosciences Divisions, Argonne National Laboratory, Argonne, Illinois; [4]Department of Biochemistry and Center for Biophysics and Computational Biology, University of Illinois, Urbana, Illinois; and [5]Department of Physics and Astronomy, Vrije Universiteit Amsterdam, Amsterdam, The Netherlands

ABSTRACT The electrostatic potential in the secondary quinone (Q_B) binding site of the reaction center (RC) of the photosynthetic bacterium *Rhodobacter sphaeroides* determines the rate and free energy change (driving force) of electron transfer to Q_B. It is controlled by the ionization states of residues in a strongly interacting cluster around the Q_B site. Reduction of the Q_B induces change of the ionization states of residues and binding of protons from the bulk. Stigmatellin, an inhibitor of the mitochondrial and photosynthetic respiratory chain, has been proven to be a unique voltage probe of the Q_B binding pocket. It binds to the Q_B site with high affinity, and the pK value of its phenolic group monitors the local electrostatic potential with high sensitivity. Investigations with different types of detergent as a model system of isolated RC revealed that the pK of stigmatellin was controlled overwhelmingly by electrostatic and slightly by hydrophobic interactions. Measurements showed a high pK value (>11) of stigmatellin in the Q_B pocket of the dark-state wild-type RC, indicating substantial negative potential. When the local electrostatics of the Q_B site was modulated by a single mutation, L213Asp→Ala, or double mutations, L213Asp-L212Glu→Ala-Ala (AA), the pK of stigmatellin dropped to 7.5 and 7.4, respectively, which corresponds to a >210 mV increase in the electrostatic potential relative to the wild-type RC. This significant pK drop ($\Delta pK > 3.5$) decreased dramatically to ($\Delta pK > 0.75$) in the RC of the compensatory mutant (AA+M44Asn→AA+M44Asp). Our results indicate that the L213Asp is the most important actor in the control of the electrostatic potential in the Q_B site of the dark-state wild-type RC, in good accordance with conclusions of former studies using theoretical calculations or light-induced charge recombination assay.

INTRODUCTION

The electrostatic potential plays a fundamental role in the structure and function of biomembranes and energy-transducing membrane proteins (1). Due to the alignment of phosphate headgroups of lipids in the membranes and water dipoles at the interface of the lipid polar region and the aqueous bulk phase, a large electrostatic potential (~300–400 mV) can be generated inside the bilayer (2). The membrane dipole potential affects the function of the RC of photosynthetic bacteria (3), the activity of the Na^+-K^+-ATPase (4), the conductance of the gramicidin channel (5), and the fusion of the human immunodeficiency virus and the target-cell membranes (6). In energy-converting proteins like photosynthetic RCs, the electron and proton transfers are under electrostatic control and the majority of molecular energy storage and retrieval processes are influenced by electrostatic interaction (7,8).

Many techniques have been worked out to measure the electric field strength or electrostatic potential in whole cells, membranes, and proteins. Patch/voltage-clamp techniques are confined to an ~1 μm^2 area cellular membranes, which corresponds to <0.1% of the surface area of an average mammalian cell. A new nanosized (30 nm) photonic voltmeter was constructed that is 1000-fold smaller than existing voltmeters and enables complete three-dimensional electric field profiling of the entire volume of living cells (9). Quantitative analysis of the electric field or electrostatic potential inside the protein demands a site-specific, accurate, and sensitive (1 mV resolution) spectroscopic method. Fast-relaxing charged and neutral paramagnetic relaxation agents (nitroxide spin labels) (10) or vibrational spectroscopy probes (11,12) can fulfill these requirements. The electrostatic potential on the protein surface can be mapped using atomic force microscopy with high resolution (0.1–0.5 nm) (13). The electrochromic responses of native dyes (chlorophyll *b* and carotenoids) in the photosynthetic membranes of green plants and purple bacteria (14,15) are often used as molecular voltmeters. However, the electrochromic voltmeter has not been commercially successful outside of photobiology because the absorption change is too small ($\Delta A < 10^{-3}$) even at very high field strengths (10^7 V/m). Much larger signals can be obtained by

Submitted July 31, 2014, and accepted for publication November 19, 2014.

*Correspondence: l.gerencser@vu.nl or pmaroti@sol.cc.u-szeged.hu

Editor: Michael Feig.

0006-3495/15/01/0379/16 $2.00

http://dx.doi.org/10.1016/j.bpj.2014.11.3463

membrane-adsorbed dyes that undergo voltage-sensitive isomerization (16).

This study describes the measurement of the electrostatic potential in the quinone (Q_B) binding pocket of the RC of the photosynthetic bacterium *Rhodobacter* (*Rb.*) *sphaeroides*. The potential controls the rate and free-energy change of the first electron transfer ($Q_A^- Q_B \rightarrow Q_A Q_B^-$) between the two electron acceptor quinones (Q_A and Q_B). It also influences the rate of proton transfer between the bulk phase and the Q_B site by adjusting the p*K* values of protonatable residues in the proton path (17,18). In addition, it controls the rate of the second interquinone electron transfer ($Q_A^- Q_B^- \rightarrow Q_A (Q_B H)^-$) by modifying the p*K* of single reduced Q_B. Whereas quinones are firmly bound to the Q_A site in each redox form (oxidized or singly reduced), they can dissociate from the Q_B binding site in oxidized or doubly reduced forms (18). Driven by absorption of two photons by the RC, the quinone in the Q_B site binds two electrons and two protons in an alternating pattern (19). The quinol ($Q_B H_2$) is more weakly bound to the Q_B site than the oxidized quinone, and therefore, it rapidly exchanges for an oxidized quinone from the pool. Studies focusing on the pH dependence of the rates and equilibrium constants of the interquinone electron transfers (17,20), the stoichiometries of proton uptake induced by the reduction of Q_B (21), vibrational spectroscopic measurements (22), the tuning of the redox midpoint potential of Q_A and Q_B by the 2-methoxy dihedral angle (23) or by site-directed mutations of nearby amino acids (8), and analysis of the system by continuum electrostatic calculations (24,25) have revealed that the decisive factor in control of the interquinone electron transfer is the electrostatic potential in the binding region. There are at least two problems with drawing conclusions about changes in the electrostatics in the Q_B pocket based on the results of these studies. First, some essential points remain controversial, especially the ionization states of the key residues L212Glu and L213Asp (22). Second, although these investigations have revealed many essential details about coupling of electron transfer to proton uptake at the Q_B site, they have shown that some nonelectrostatic mechanisms, such as conformational gating (26,27) and dynamics of the protein (24,28,29), also help to control interquinone electron transfer.

Systematic site-directed mutagenesis studies on the ionizable residues around the Q_B site in the RC of *Rb. sphaeroides* and its highly homologous strain *Rb. capsulatus* identified residues that play an important role in electron and proton transfer to the Q_B. The selected ionizable amino acids were replaced by nonionizable ones and the characteristic parameters of the function of the quinone acceptor complex, like the rates (k_{BP} or k_{AP}) of charge recombination ($P^+ Q_B^- \rightarrow PQ_B$) or ($P^+ Q_A^- \rightarrow PQ_A$) between the oxidized bacteriochlorophyll dimer (P^+) and the reduced quinones (Q_B^- or Q_A^-), the rates ($k_{AB}(1)$ and $k_{AB}(2)$) and free energy changes (ΔG^1_{AB} and ΔG^2_{AB}) of first and second interquinone electron transfer, and the rates and stoichiometries of first ($k_H(1)$, (H^+/RC) (1)) and second ($k_H(2)$, (H^+/RC) (2)) proton uptake were measured. These assays revealed that the L212Glu and L213Asp residues were key players in the function of the quinone acceptor complex of wild-type (WT) RC. The replacement of these amino acids by nonprotonatable alanines (L212Glu-L213Asp → Ala-Ala (AA double mutation)) made the strain photoincompetent, with a highly increased doubling time (200 h vs. 8 h for WT (30)). The photosynthetic incompetence of the strain was related to the highly decelerated rate of proton transfer to the Q_B in the mutant RC, expressed by $k_{AB}(2)$ (2 s^{-1} vs. 2000 s^{-1} at pH 7.0 (31)) together with $k_{AB}(1)$ (150 s^{-1} vs. 5×10^5 s^{-1} (30)) and k_{BP} (0.08 s^{-1} vs. 0.75 s^{-1} (32)). No flash-induced proton binding was observed in the mutant RC above pH 9.0 (33,34), although the WT RC exhibited relatively high proton binding stoichiometries (0.2–0.3) upon PQ_A^- or PQ_B^- formation in the alkaline pH range (21). The crystal structure of AA mutant RC (Protein Data Bank (PDB) ID 1K6N) revealed significant changes of the Q_B position, an expanded cavity, and an extra water molecule around the L212Ala and L213Ala residues (35). The single mutation L212Glu → Ala resulted in less dramatic changes: the strain remained photocompetent, with a doubling time of 8 h (34). The rate constants of $k_{AB}(2)$ and $k_H(2)$ decreased by a factor of only 2.5 relative to those in WT, and to our surprise, k_{BP} increased to 4 s^{-1}. The pH dependence of flash-induced proton binding stoichiometry was identical to that in the AA mutant RC (33,36). The L213Asp → Ala single mutation has not yet been characterized, but the highly homologous L213Asp → Asn mutant is described in the literature (37,38). It turned out that L213Asp → Asn was highly similar to the AA double mutation: the strain was photoincompetent, and the rate constants $k_{AB}(1)$, $k_{AB}(2)$ (depending on $k_H(2)$), and k_{BP} decreased by factors of 10, 1000 (both at pH 7.0), and 17, respectively, relative to that in WT RC. The highly decelerated rate of proton transfer in AA double mutant RC could be accelerated by a third, revertant mutation, where a nonionizable amino acid in the Q_B environment is replaced, usually by an ionized residue. The mutations of AA+M44Asn → AA+M44Asp, AA+M233Arg → AA+M233Leu, and AA+L217Arg → AA+L217Cys restored the photosynthetic activity, and the values of k_{BP} (0.15 s^{-1} (31), 0.2 s^{-1} (31,32), and 0.9 s^{-1} (39)), $k_{AB}(2)$ (50 s^{-1} (31), 20 s^{-1} (31), and 10 s^{-1} (39), all at pH 7.0) increased relative to that in the AA mutant RC and became closer to that in the WT RC. The proton stoichiometry binding pattern in AA+M44Asn → AA+M44Asp mutant RC was identical to that in the AA mutant RC (33). However, in the AA+M249Ala → AA+M249Tyr (AAY) mutant RC, where the mutated M249Ala residue is the structural equivalent of L213Asp in the Q_A binding domain, the proton stoichiometry values were restored to those in the WT RC (40).

For the positions of the mutated residues in the environment of the Q_A and Q_B sites in the *Rb. sphaeroides* RC, see Fig. S1 in the Supporting Material. Note the difference between the amino acid sequence of the third compensatory mutation in *Rb. capsulatus* AA+M43Asn→AA+M43Asp, AA+M231Arg→AA+M231Leu, and AA+M247Ala→AA+M247Tyr and that in *Rb. sphaeroides* AA+M44Asn→AA+M44Asp, AA+M233Arg→AA+M233Leu and AA+M249Ala→AA+M249Tyr.

The differences in the highly complex pattern of proton binding in the RC between different mutants and the WT cannot be predicted based on simple changes in the binding-site electrostatics due to addition or removal of charges at the sites of mutation(s) (41). Thus, there is a substantial need to measure directly the electrostatic potential inside the RC with high spatial resolution. In this study, the electrostatic potential in the Q_B binding site was monitored by measurement of the p*K* of the phenolic group of antibiotic stigmatellin.

Stigmatellin is a potent electron transfer inhibitor in several redox proteins of bioenergetic membranes like bacterial photosynthetic RCs (42), photosystem II of higher plants (43), and cytochrome bc_1 complex of the mitochondrial or photosynthetic respiratory chain (44). Although the reported dissociation constant (K_S) and inhibition constant (I_{50}) of stigmatellin from the Q_B site of the RC cover a broad range (K_S = 50 nM in isolated RC (45) and 165 nM in detergent-free RC (46), I_{50} = 1.5 μM in the cytochrome bc_1 free membrane of mutant *Rb. sphaeroides* (42), and K_S = 0.37 μM in the native membrane of *Rb. capsulatus* (47)), they show very tight binding. Due to the H-bonds between the chromone headgroup of stigmatellin and the Q_B pocket of RC, stigmatellin inhibits turnover of the RC even at equimolar concentrations.

High-resolution crystal structure of the RC with bound stigmatellin at the Q_B site is not yet available for *Rb. sphaeroides*, but the corresponding structure has been resolved for the nonsulfur purple bacterium *Blastochloris viridis* (48,49) (Fig. 1). Comparing the chemical structures and binding positions of the quinones and the antibiotic stigmatellin, it appears that stigmatellin resembles the protonated semiquinone at lower pH (<8) and the semiquinone anion radical at higher pH (>10). These quinone redox states are essential intermediates in the quinone reduction photocycle (17). However, the protonated semiquinone is not readily accessible by direct spectroscopic and kinetics methods (7), so stigmatellin may provide some insight into the modes of binding and interactions of semiquinones in the photocycle of the RC.

Preliminary studies indicate that the protonation state of the phenolic group of stigmatellin (the pK_a value) monitors the electrostatic potential around the Q_B binding site of the RC (50,51). However, the p*K* value can be sensitive also to the nonelectrostatic interaction between stigmatellin and the environment. This study demonstrates how sigmatellin can be used to probe the local electrostatics in the Q_B site.

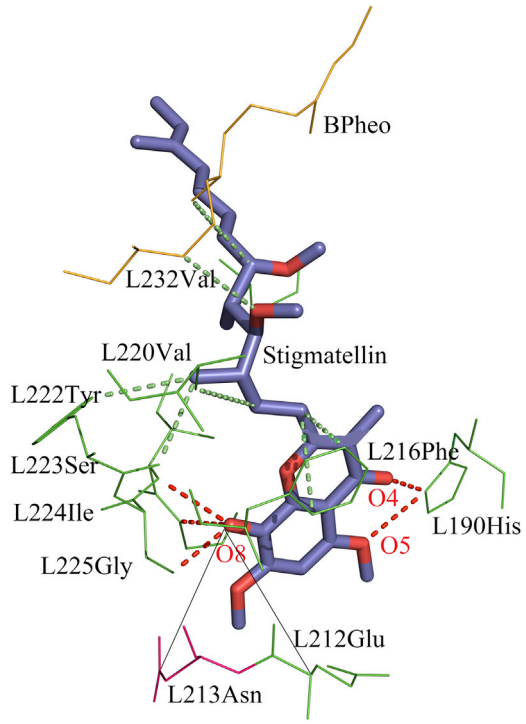

FIGURE 1 Stigmatellin in the Q_B binding site of the RC from *Blastochloris viridis* (from PDB ID 2JBL (updated from the previous version, 4PRC)) (48,49). Stabilizing H-bond interactions between the chromone headgroup of the stigmatellin and the RC (stig O4 ↔ L190His Nδ, stig O5 ↔ L190His Nδ, stig O8 ↔ L224Ile N, stig O8 ↔ L225 Gly N, and stig O8 ↔ L223Ser Oγ (*red dashed lines*)) and nonbonded interactions between the stigmatellin side chain and the RC (*green dashed lines*). The distance between the carboxylic oxygen of L212Glu and that of L213Asp in *Rb. sphaeroides* RC and O8 of the stigmatellin is 7 Å.

MATERIALS AND METHODS

Site-directed mutagenesis and growth conditions

The *Rb. sphaeroides* AA double mutant and its compensatory mutants (AAY, AA+M44Asn→AA+M44Asp, AA+L217Arg→AA+L217Cys, and AA+M233Arg→AA+M233Leu) were designed and characterized first in the homologous strain, *Rb. capsulatus* (30). The cells of *Rb. sphaeroides* were grown in Erlenmeyer flasks filled to 50% of the total volume with malate yeast medium supplemented with kanamycin (20 μg/mL) and tetracycline (2 μg/mL). The cultures were grown in the dark at 30°C on a gyratory shaker (100 rpm).

RC and chemicals

Purification of the RC from WT (52) and different mutant strains (53) of *Rb. sphaeroides* has been previously described. The protein/pigment ratio (purity) of the RC (A_{280}/A_{802}) was <1.3. After preparation, the RC contained 1 Q_{10}/RC in the Q_A site and ~0.5 Q_{10}/RC in the Q_B site.

The pH of the isolated RC or detergent solution was measured by calibrated glass electrodes and adjusted by addition of small (1–5 μL) amounts of concentrated HCl or NaOH solutions in the presence of buffers (Mes, Mops, Tris, Ches, Caps) depending on pH range. The 4 mM stock solution of stigmatellin (Fluka, St. Louis, MO) was prepared with ethanol.

Steady-state absorption measurement

The steady-state absorption spectrum of the stigmatellin was measured with a dual-beam (sample and reference beams) ultraviolet-visible (UV-vis) spectrophotometer (model 4A, Unicam, Cambridge, UK). The small absorption of stigmatellin ($A < 10^{-2}$) had to be detected in a background of large absorption ($A > 1$) of the RC in the UV range where light scattering was substantial. Any modification of the pH resulted in a change of the absorption spectrum of the RC, since a small fraction of the protein precipitated during the pH adjustment, which caused increased light scattering. To reduce light scattering, the precipitated RC was removed with centrifugation and near-field observation was used for absorption measurements. Changes in the absorption spectrum of stigmatellin were detected by removal of the large absorption background of the RC. The RC solution served as a reference for the stigmatellin. (The baseline was recorded using two identical RC solutions. Stigmatellin dissolved in ethanol was added to the RC solution in the sample beam (sample) and an identical volume of ethanol was added to the RC solution in the reference beam (reference).) All measurements were carried out at 25°C.

Model calculations

Model calculations of the energetics of stigmatellin binding, protonation equilibrium, and transitions between water and detergent phase and ionic screening of micelles with electrolyte were carried out using MathCad 13.0 based on mathematical models described in Appendices A–C.

RESULTS

Characterization of the protonation state of stigmatellin

The steady-state absorption spectrum of aqueous solution of stigmatellin follows the protonation-state change of the inhibitor with high sensitivity. The observed absorption spectrum is a linear combination of the spectra of deprotonated and protonated forms of the phenolic group of stigmatellin with weighting factors set by the prevailing pH (Fig. 2, *left*). It showed characteristic bands at 272 nm (strong, narrow, and part of the complex UV band) and at 340 nm (much weaker, broader, and well isolated). Both bands are very sensitive to pH in the interval close to the pK value of the phenolic group. The absorption spectra recorded at different pH values showed an isosbestic point around 300 nm, indicating the interconversion of two absorbing species with maxima at 272 and 340 nm. As the pH was increased, the 340 nm band disappeared completely, and the 272 nm band increased significantly. By comparing the absorption spectra of the protonated and unprotonated forms of stigmatellin, the absorption peak at 272 nm can be calibrated: $\varepsilon_{272\ \mathrm{nm}}(\mathrm{deprotonated}) = 54\ \mathrm{mM}^{-1}\cdot\mathrm{cm}^{-1}$ and $\varepsilon_{272\ \mathrm{nm}}(\mathrm{protonated}) = 44\ \mathrm{mM}^{-1}\cdot\mathrm{cm}^{-1}$. These values can be used to calibrate the ratio of the deprotonated to protonated form in buffer solution.

Electrostatic and hydrophobic interactions modify the pK of stigmatellin in detergent solutions

The pH titration of free stigmatellin can be well described by the Henderson-Hasselbalch curve for a single protonatable group. The pK of the phenolic group of stigmatellin was $\mathrm{p}K_w = 9.1$ in water (in 50 mM NaCl), which increased only slightly (~0.2–0.3 pH unit) in the presence of low buffer concentration (5-5 mM Mops, Tris, Caps, and Ches) (data not shown). However, addition of zwitterionic lauryldimethylamine N-oxide (LDAO) detergent caused the pK value to increase significantly. For example, increasing the concentration of LDAO from 0.003% (~0.13 mM) to 0.04% (~1.74 mM) in the aqueous buffer solution (Fig. 2, *right*) increases the pK value from 9.48 to 10.1. The pK of stigmatellin in aqueous detergent solution depends on the type (anionic, neutral, zwitterionic, or cationic) and concentration of the detergent (Fig. 3). The results of calibration tests in model systems may allow estimation of the in situ electrostatic potential in the protein environment.

When the detergent concentration was increased, the pK of stigmatellin determined in aqueous buffer solution (9.3–9.4) monotonically decreased with cationic detergents and

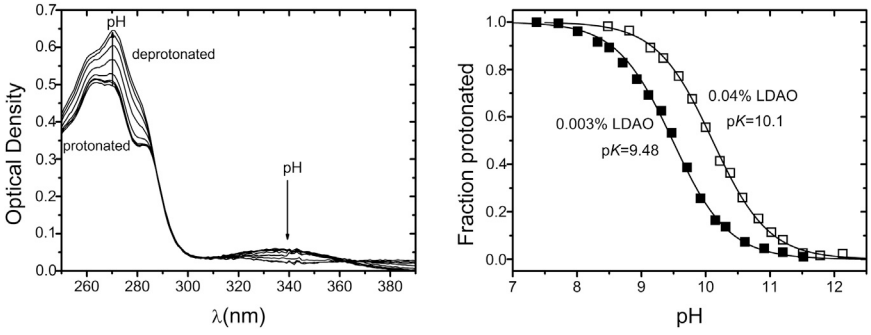

FIGURE 2 (*Left*) Steady-state absorption spectrum of stigmatellin at different pH values. The peak at 272 nm increases with increasing pH (from 6.8 to 12.05), whereas that at 340 nm decreases with increasing pH (see *arrows*). Conditions: 11 μM stigmatellin, 0.03% Triton X-100, and 1-1 mM Tris, Ches, and Caps buffers. (*Right*) pH titration of stigmatellin in aqueous buffer solution of 0.003% (~0.13 mM) and 0.04% (~1.74 mM) LDAO. The pK of stigmatellin was determined from the fit of the raw data with the Henderson-Hasselbalch equation. Conditions: 5 μM stigmatellin and 5-5 mM Tris, Ches, and Caps buffers.

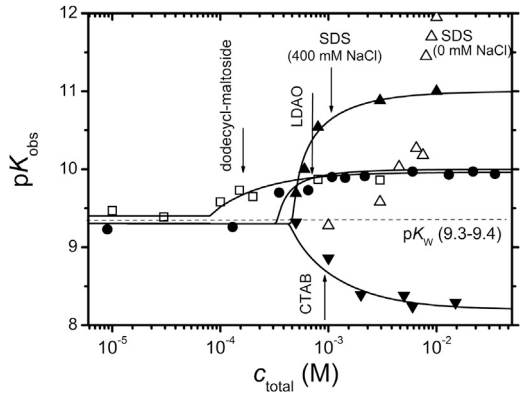

FIGURE 3 Detergent titration of the pK of stigmatellin in cationic (CTAB, cetyl trimethylammonium bromide), neutral (dodecyl-maltoside), zwitterionic (LDAO), and anionic (SDS) detergents. Each pK value was derived from the fit of the pH dependence of the protonation of stigmatellin with the Henderson-Hasselbalch equation. Note the sudden changes at the CMC values of the detergents (*arrows*). In the case of SDS, the pK was extremely high; therefore, it was not determined precisely. The fitting curves were derived from the model described in Appendix A. Conditions: 10 μM stigmatellin, 5-5 mM Tris, Ches, and Caps buffers.

increased with all other types of detergents. It leveled off above the critical micelle concentrations (CMC) for all detergents. The only exception was sodium dodecyl sulfate (SDS), where the pK value showed such a dramatic increase that no plateau was observed within the measurable pH range. Below the CMC, the added detergents dissolve in the solution as a monomer, and little or no micelle formation is observed. Above the CMC, however, the detergent monomers associate to micelles. Thus, the observed transition and saturation phases of the stigmatellin pK as a function of detergent concentration refer to a mixed solution of detergent monomers and micelles and a homogeneous solution of micelles, respectively (see Appendix A). The change in the pK of stigmatellin in micelles (pK_m) relative to that in water, $\Delta pK = pK_m - pK_w$, is indicated in Table 1. The shape of the pK change as a function of detergent concentration is defined by the hydrophobic interaction between stigmatellin and the micelle, whereas the magnitude of the pK change is modulated by the electrostatic interaction depending on the type of the detergent.

The pK increase induced by the hydrophobic effect is enhanced in anionic detergent and compensated in cationic detergent. The sign of the change clearly demonstrates the dominant role of the electrostatic interaction, whereas the relatively small upward ΔpK of 0.4–0.7 pH units experienced in neutral detergents (dodecyl-maltoside and LDAO (at high pH)) provides an estimate of the magnitude of the hydrophobic interaction.

The relatively large free energy differences of transition of stigmatellin between the micellar and aqueous phases (200–500 meV, see Table 1) indicate a strong preference of stigmatellin for the hydrophobic environment over the aqueous phase. Whether the protonated or the deprotonated form of stigmatellin has a larger affinity for the hydrophobic phase depends on the type of detergent.

If stigmatellin is embedded in an anionic micelle, the electrostatic interaction with the micelle leads to a pK_m that is so high that a full pH titration would need to extend beyond pH 12, which is the measurement limit. However, by increasing the ionic strength of the solution, the surface electrostatic potential of the micelle can be decreased (54) and the pK_m value of stigmatellin can be brought into a lower, directly measurable pH range. Increasing the ionic strength from 0.09 M to 0.64 M causes the observed pK value to drop from 11.6 to 10.95 (Fig. 4).

Stigmatellin bound at the Q_B binding site of the RC

Stigmatellin binding to the Q_B site of the RC alters the absorption spectrum of the fully protonated form of stigmatellin significantly. For that reason, another, more reliable and sensitive spectroscopic measure of the deprotonation, the ratio $(A_{278} - A_{300})/(A_{287} - A_{300})$, was introduced (Fig. 5). The difference of the absorption spectra is localized in a narrow region around 272 nm and does not affect the absorption at characteristic wavelengths of the spectroscopic ratio (278 nm, 287 nm, and 300 nm). A_{278} monitors the protonation change of the stigmatellin, whereas A_{287} and A_{300} are necessary to normalize the concentration of stigmatellin. If stigmatellin is not bound to the Q_B site, then there is no difference between the pK values derived from the change of the 272 nm (or 340 nm) peak and the spectroscopic ratio $(A_{278} - A_{300})/(A_{287} - A_{300})$.

TABLE 1 Characteristics of energetics of stigmatellin in micelles from different types of detergent

		Micelle formation		Stigmatellin in micelle			
Detergent	Type	Aggregation number, n	CMC (M)	ΔG_S^0 (meV)	ΔG_{SH}^0 (meV)	pK_m	$\Delta pK = pK_m - pK_w$[a]
Dodecyl-maltoside	Neutral	61	1.6×10^{-4}	264	290	9.84	+0.44
LDAO	Zwitterionic (neutral at high pH)	76	7.0×10^{-4}	265	307	10.0	+0.71
CTAB	Cationic	100	9.0×10^{-4}	280	215	8.2	–1.1
SDS (no salt)	Anionic	61	1.0×10^{-2}	185	481	14.3[b]	+5.02
SDS + 400 mM NaCl			1.0×10^{-3}	220	321	11.0	+1.72

For definitions of ΔG_S^0 and ΔG_{SH}^0, see Fig. A1 in Appendix A.
[a]$pK_w = 9.3$–9.4, depending on the ionic strength of the buffer solution.
[b]Extrapolated value (see Eq. 1).

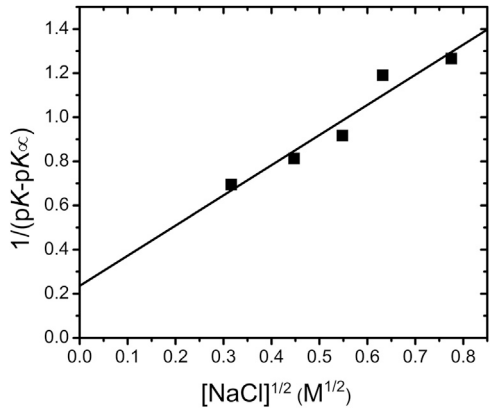

FIGURE 4 Observed pK shift of 10 μM stigmatellin in aqueous solution of 15 mM SDS due to the ionic screening of the micelle surface potential by different concentrations of NaCl. According to Eq. 1, the linear fit of the plot of $1/(pK - pK_\infty)$ values as a function of $[NaCl]^{1/2}$ provides the fitting parameters of $pK_\infty = 10.16$ and $\psi_0 = -246$ mV (for definitions, see Appendix B). The fitting parameters can be directly derived from the y intercept (0.24) and from the slope (1.35).

The pK value of stigmatellin bound to the Q_B site of RC (pK_{QB}) cannot be determined by a classical pH titration, because any adjustment of the solution pH induces significant absorption change due to protein denaturation (see Materials and Methods). The following method proved more efficient and reliable: the RC solution was titrated by stigmatellin at several fixed pH values, and at each stigmatellin concentration, the spectroscopic ratio $(A_{278} - A_{300})/(A_{287} - A_{300})$ was determined. By gradually increasing the stigmatellin/RC ratio, the stigmatellin is distributed into different phases of the micellar solution of RC. It can be either bound to the Q_B site or attached to the RC surface or the free micelle. At a low stigmatellin/RC ratio, it binds preferentially to the Q_B pocket with less attachment to the surface of the RC. Upon increasing the stigmatellin concentration, the Q_B site becomes saturated and the stigmatellin accumulates in free micelles and at the surface of the RC. Any changes in the spectroscopic ratio during the stigmatellin titration refer to distinct pK values of the inhibitor in the different phases. However, constant titration values at a given pH might reflect different scenarios, for instance, localization of stigmatellin in a single phase, or identical pK values of stigmatellin in the different phases that are close to the pH value ($|pK - pH| < 1.0$), or distinct pK values that are significantly different from the pH ($|pK - pH| > 1.5$).

WT RC

In the presence of WT RC (solubilized in 0.04% LDAO), there was no or very little change in the spectroscopic ratio $(A_{278} - A_{300})/(A_{287} - A_{300})$ as a function of stigmatellin concentration at all pH values, but a significant increase in this ratio with increasing pH at all stigmatellin concentrations (Fig. 6). However, some small pH-dependent differences could be clearly recognized between the stigmatellin binding titration data measured at different pH values: whereas the titration values were definitely constant at low (7.7) and high pH (>10.5), they showed a small increase in the intermediate pH range (pH 9–10) with increasing stigmatellin concentration. These small changes in the spectroscopic ratio indicated that the pK values of stigmatellin bound to the

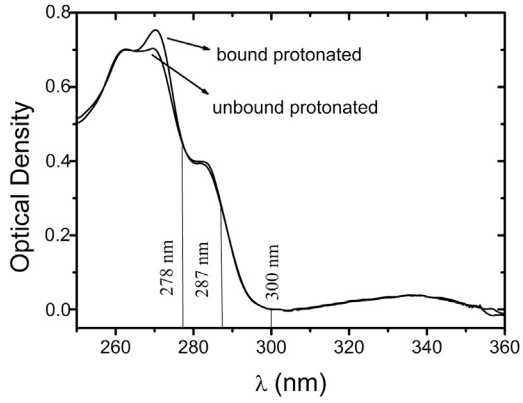

FIGURE 5 Modification of the absorption spectrum of the protonated stigmatellin due to its binding to the Q_B site of the RC. The large absorption background of the RC was subtracted by addition of the same amount of RC (3.8 μM) to the reference and to the sample. Initially, the RC was in large excess to the stigmatellin (3.8 μM vs. 1 μM), so the measured absorption spectrum refers to the stigmatellin that is bound to the Q_B site. Addition of 5 μM stigmatellin to the sample and to the reference in the next step caused the Q_B site to become saturated. A new baseline was recorded, and by further addition of 1 μM stigmatellin to the sample, the measured absorption spectrum refers to the unbound stigmatellin in the micellar phase. Conditions: 0.04% LDAO, 10 mM Tris, pH 7.9.

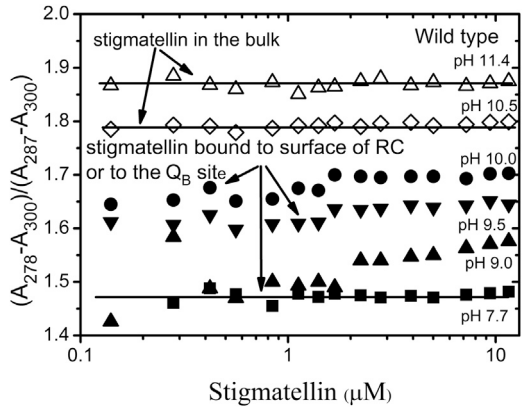

FIGURE 6 The pK of stigmatellin in the Q_B site of the WT RC (pK_{QB}) was estimated from stigmatellin titrations at different pH values. The titration curves showed only small deviations from a constant value, indicating that the pK of stigmatellin is the same in the different phases (in the Q_B pocket or on the surface of the RC (*solid symbols*) and in the micellar solution (*open symbols*)). The assay has serious limitations at higher pH (>10.5), where the binding affinity of stigmatellin for the Q_B site drops sharply. As a consequence, only a lower limit is given for pK_{QB} (>11). Conditions: 3 μM RC, 0.04% LDAO, 10 mM Tris, and 20-20 mM Ches and Caps buffers.

Q_B site and to the surface of the RC had to be close ($\Delta pK < 1$) and/or that the stigmatellin binding capacity of the surface of RC was significant. The titration data measured at higher pH (>10.5) did not show any change, because at this pH the stigmatellin was not bound to either the Q_B site or the RC surface. By increasing the concentration of LDAO to 0.5% in the RC solution, the complexity of the stigmatellin titrations pattern disappeared (not shown). The stigmatellin did not bind to the RC surface at all, and the relatively large pK difference (1–1.5) between stigmatellin bound to the Q_B site and stigmatellin dissolved in micelle solution was expected to become visible. Unfortunately, the high LDAO concentration decreased the apparent binding affinity of the stigmatellin to the Q_B site, so no binding was observed above pH 10.0, where the stigmatellin binding affinity is even lower than below pH 10.0. Due to these experimental limitations in the LDAO-solubilized RC, only a rough estimate of the pK values of stigmatellin bound to the Q_B site (>11.0) and attached to the surface of the RC (10.5–10.75) could be obtained for the WT RC. By replacing the LDAO with a cationic detergent, the pK_m value can be decreased significantly and the pK_{QB} value might be determined with higher accuracy.

RC with single, double, and compensatory mutations

The titration pattern in the AA double mutant RC is strikingly different from that found in the WT RC (Fig. 7, *left*). The changes in the local electrostatic interactions in the vicinity of the Q_B site due to the mutation are shown by a significant drop in stigmatellin pK_{QB}, determined from simulations of the measured data derived from the model described in Appendix C. At pH 9.0, the spectroscopic ratio at low stigmatellin concentration was maximal in the double mutant RC, whereas it was minimal in the WT RC (compare Figs. 6 and 7). In the mutant RC, the spectroscopic ratios showed a dramatic drop during stigmatellin titration at a given pH (Fig. 7, *left*). The ratio saturated at a level similar to the saturation level for the WT RC, as the pK value of stigmatellin dissolved in the micellar phase is independent of the mutation in the protein. Due to the mutation, the pK_{QB} value (7.4) falls in the pH range where stigmatellin binding is strong, and its difference from that found in the micelle ($pK_m \approx 10$) became significant ($\Delta pK \sim 2.6$). These factors make the titration data of the mutant RC demonstratively different from that of the WT RC. In addition, due to the large drop in stigmatellin pK_{QB}, we had to select the lowest pH values of the measurement in the pH range (<6.5) where the RC is poorly solubilized in 0.04% LDAO (55). To circumvent the solubilization problem of AA mutant RC, the concentration of LDAO was set to 0.5% at all pH values during the stigmatellin titration assay (Fig. 7, *left*), but it was kept at 0.03% for the quinone binding assay (see below) at pH 8.15 (Fig. 7, *right*).

To confirm that the low pK_{QB} value (7.4) of the stigmatellin in the AA double mutant reports on only the stigmatellin bound to the Q_B site, stigmatellin titrations were carried out at different initial (UQ_6) concentrations (Fig. 7, *right*). As a result of competitive binding of stigmatellin and quinone to the Q_B site, the stigmatellin is removed from the Q_B pocket and accumulates in the micellar solution. Consequently, the predominantly deprotonated form found initially in the Q_B pocket becomes protonated at the same pH (8.15), showing that the pK increases as stigmatellin moves to the micellar phase. A dramatic drop in the spectroscopic ratio at low stigmatellin concentration was observed with increasing initial UQ_6 concentration. This result confirms unambiguously that the stigmatellin characterized with low pK (7.4) was bound to the Q_B pocket and it can be replaced by UQ_6 (Fig. 8).

The severely decelerated proton transfer in the AA mutant RC can be partially or fully restored to its original rate by third-site compensatory mutations in the vicinity of the Q_B binding pocket (56,57). Is it possible to restore the high pK_{QB} value of stigmatellin experienced in WT RC with a compensatory mutation in the AA mutant RC? Yes it is, but the magnitude of the pK increase depends highly on the position of the compensatory mutation. In

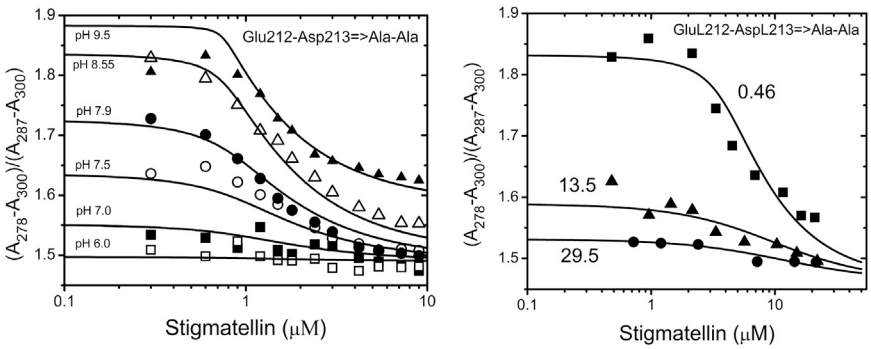

FIGURE 7 (*Left*) The pK_{QB} value of stigmatellin in the case of the RC from double mutant strain AA was determined using the stigmatellin binding titration assay described in the Fig. 6 legend.Conditions: 0.8 μM RC, 0.5% LDAO, 10-10 mM Mes, Mops, and Tris buffers, and 20-20 mM Ches and Caps buffers. The fit parameters are $K_d^S = 0.9$ nM and $pK_{QB} = 7.4$, and $pK_m = 10$ was taken from Fig. 3. (*Right*) Stigmatellin titrations with different initial quinone content at pH 8.15. Stigmatellin bound to the Q_B site is deprotonated (the spectroscopic ratio is high at low stigmatellin concentration), and it becomes protonated in micellar solution when it is removed from the Q_B site by increasing the $[UQ_6]/[RC]$ ratio, as indicated by the decrease in the spectroscopic ratio. The simulations were derived from the model described in Appendix C. Conditions: 1.5 μM RC, 0.03% LDAO, pH 8.15. $[UQ_6]/[RC]$ ratios are indicated on each titration curve. The fit parameters are $K_Q = 0.78$ μM and $K_d^S = 1.33$ nM with parameters $pK_{QB} = 7.4$ and $pK_m = 10$ obtained from Figs. 7 left and 3, respectively.

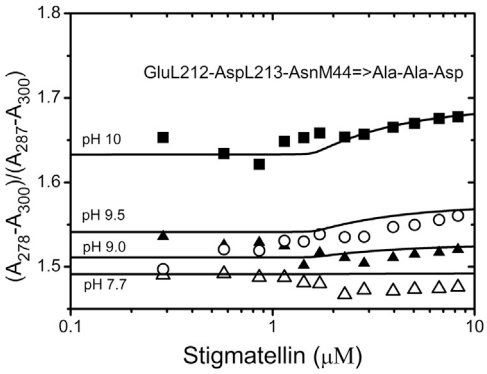

FIGURE 8 Stigmatellin titration assay with RC from the compensatory mutation (L212Glu-L213Asp-M44Asn→Ala-Ala-M44Asp) of the AA mutant. The titration data at a given pH showed only a small increase, implying that the stigmatellin pK is similar in the different phases. As a result of the compensatory mutation (M44Asn→Asp), the pK_{QB} value was increased relative to that found in the AA mutant, approaching that of the WT. Fit parameters were pK_{QB} = 10.25 and K_d^S = 10 nM and pK_m = 10 was taken from Fig. 3. Conditions are the same as in Fig. 7, *left*, except for the concentration of RC, which was 1.6 μM.

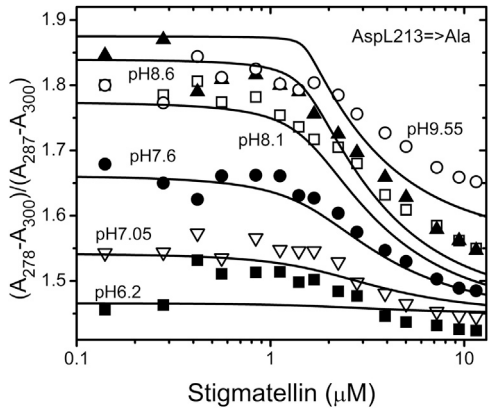

FIGURE 9 The stigmatellin titration pattern with the RC from single-mutation AspL213→Ala. Fitting parameters are pK_{QB} = 7.5 and K_d^S = 1.45 nM, and pK_m = 10 was taken from Fig. 3. Conditions are the same as in Fig. 7, *left*, except that the concentration of RC was 1.5 μM.

the AA+M44Asn→AA+M44Asp suppressor mutant RC, the stigmatellin titration data were nearly constant at a given pH and resembled those of the WT RC (Fig. 8). A pK_{QB} value of 10.25 was derived from the simulations. The introduction of a negative charge at a distance of 4 Å from Q_B (M44Asn→Asp) restored the high negative electrostatic potential in the Q_B site detected in the WT RC. Using other suppressor mutants of the AA mutant (L217Arg→Cys and M233Arg→Leu), similar recovery of the electrostatic potential (9.5 < pK_{QB} < 10.5) was obtained (data not shown). However, in the AAY triple mutant, where the stoichiometry of proton uptake at high pH was fully restored (40), surprisingly, the electrostatic potential as determined by stigmatellin pK did not recover to the WT value and remained close (~7.5) to that in the AA mutant RC (data not shown).

The results with the single mutant L213Asp→Ala (Fig. 9) are highly similar to those obtained in the AA mutant (Fig. 7). The dramatic drop in the pK_{QB} value of stigmatellin due to this single mutation (ΔpK ~ 3.5) highlights the crucial role of residue L213Asp in setting the prevailing electrostatic potential at the Q_B binding site of the WT RC. In the single mutant L212Glu→Ala RC, the stigmatellin titration curves resemble that found for WT RC, and for the corresponding pK_{QB} value only a rough estimate was given (>10.5) (data not shown).

DISCUSSION

Probe of hydrophobic and electrostatic interaction

The antibiotic stigmatellin has proved to be an ideal candidate to probe the electrostatics at the Q_B site. It binds to the Q_B site with high affinity, the electric potential change can be detected from its pK shift with straightforward calibration and high sensitivity, and the pK shift can be determined by a steady-state optical spectroscopic method.

Comparison of the stigmatellin pK values in different detergents demonstrated that the pK of the phenolic group was slightly modified by hydrophobic interactions. The value of 9.3–9.4 measured in water was shifted in neutral detergents, for example, to 10.0 in LDAO or to 9.84 in dodecyl maltoside (Table 1). The shape of the pK change as a function of the concentration of neutral detergents indicates clearly that it is not the number of detergent monomers but the formation of the micelles that is responsible for the pK change. On one hand, the absence of any pK increase with increasing detergent concentration below the CMC value indicates that either the stigmatellin does not bind to monomers or the binding has no hydrophobic contribution. On the other hand, a significant increase in the pK occurs close to the CMC values (Fig. 3), reflecting the transition of the stigmatellin from the aqueous phase to the micellar phase. Thus, the stigmatellin with increased pK is localized in the interior of the micelle, and the pK is controlled by hydrophobic interactions.

The obtained pK shows much more dramatic changes when electrostatic interactions are introduced by adding either anionic or cationic detergent. The electrostatic interactions can be well calibrated given 1 pH unit/59 mV at 25°C. Based on the Debye-Hückel theory of ionic solutions, the central ion is the micelle, which is modeled by a conducting sphere surrounded by dissociated ions of salts. Since the electrostatic potential inside the conducting sphere is equal to that at the surface, so the surface potential of the conducting sphere corresponds to the

potential that is being probed by the stigmatellin inside the micelle. The decrease of the observed pK can be related to the increase in the salt concentration as follows (see Appendix B):

$$\frac{1}{\mathrm{p}K - \mathrm{p}K_\infty} = -\frac{59\ \mathrm{mV}}{\psi_0} - \frac{59\ \mathrm{mV}}{\psi_0} \times 5.52 \times \sqrt{c} \times \frac{1}{\sqrt{\mathrm{M}}}, \quad (1)$$

where $\mathrm{p}K_\infty$ is the pK of the stigmatellin in the absence of surface potential at $c \rightarrow \infty$ and ψ_0 is the surface potential of the SDS micelle in the absence of screening by salt ($c = 0$).

By taking $\mathrm{p}K_\infty = 10.16$ (in good agreement with pK values measured in hydrophobic environments of neutral micelles (see Fig. 3)), the observed pKs at different NaCl concentrations yielded a linear plot of $1/(\mathrm{p}K - \mathrm{p}K_\infty)$ versus $c^{1/2}$ according to Eq. 1 (Fig. 4). The ratio of the slope and y intercept (5.63) was very close to the value of 5.52 predicted by theory (see Eq. 1). From the y intercept ($-59\ \mathrm{mV}/\psi_0 = 0.24$), the surface potential in the absence of ionic screening, ψ_0, can be calculated as –246 mV. According to the theoretical calculation on a conducting-sphere model system (see Eq. A15 in Appendix B), which assumes that 60 elementary charges in the SDS micelle are produced by dissociation of the Na^+ ions from the detergents, one would get a surface potential of $\psi_0 =$ –635 mV. The much smaller measured value indicates either that the Na^+ dissociation is not complete in the presence of stigmatellin in the micelle or that the stigmatellin breaks the spherical symmetry of the charge distribution. The pK of stigmatellin ($\mathrm{p}K_0 = 14.3$) in salt-free solution ($c = 0$) also can be derived from Eq. 1 using $\psi_0 =$ –246 mV, i.e., the pK of stigmatellin in SDS micelles can change in a wide range from 14.3 to 10.16 upon salt titration.

The slope and y intercept of the fit and the reasonable parameters of the Debye-Hückel theory show that the phenolic group of the stigmatellin can be used as a molecular voltmeter. The observed shift of the pK of stigmatellin can be directly related to the actual electrostatic potential at the site of the phenolic group.

The inhibition at close-to-equimolar concentrations of RC and stigmatellin is due to the strong H-bonds of the chromone headgroup of stigmatellin anchored to the amino acids of the Q_B pocket and not to the conformations and interactions of the flexible tail. At higher pH values (>10.5), however, the affinity of binding to RC drops and the change of the spectroscopic ratio characteristic to the titration of stigmatellin bound to RC shifts to below the sensitivity threshold of the absorption measurement. The observed changes of the dissociation constant in the WT RC in the alkaline pH range can be attributed to slight modifications of the H-bond configurations, which are sensitive to the binding geometry and/or to changes in the protonation state of the O4H group of the stigmatellin.

An additional advantage of stigmatellin is its close structural and functional similarity to the semiquinone of the native Q_B. The protonated stigmatellin resembles the nonanionic (protonated, $QH^\bullet$) semiquinone, whereas the anionic radical semiquinone is similar to deprotonated stigmatellin. The protonated semiquinone is an important intermediate in the reduction of quinone to dihydroquinone at the Q_B site, but $QH^\bullet$ is not readily detectable by direct spectroscopic methods (58). The resemblance of $QH^\bullet$ to stigmatellin in terms of chemical structure and binding properties may provide insight into the modes of binding and interactions of semiquinones with RC during the photocycle. The semiquinone is bound to the proximal position in the Q_B site (Fig. 1), whereas the quinone may (59) or may not (27,60) be found in a distal position. Since stigmatellin binds to the proximal position even in the dark state of the RC, it provides a suitable model for the transiently formed semiquinone in the proximal position.

Electrostatics in the Q_B domain

Although light excitation of the RC generates significant perturbation of the electrostatics at the Q_B site and has important physiological consequences, this study deals with mapping the electrostatic potential only in the dark state of the RC. The local electrostatic potential in the Q_B binding site is the sum of many individual contributions, including a substantially positive potential from the peptide backbone (61) and the non-heme iron that is partially offset by the ionization of buried acidic groups (25,62); therefore, the electrostatic interactions in this domain are very complex (7).

The electrostatic potential at the Q_B site is modified by the distribution of the ionization states in the cluster of protonatable groups near the Q_B in addition to many small contributions from more weakly coupled distant residues. The most prominent acidic residues in the Q_B domain are L212Glu, L213Asp, and L210Asp, whose ionization states can strongly modify the resultant electrostatic potential. Because of the strong interactions in the cluster, the charge distribution cannot be predicted simply from the pK values of residues either determined in aqueous solution, where no electrostatic interactions are assumed (so-called intrinsic pK), or estimated individually in the protein environment. The cluster can be viewed as one group with a nonclassic titration curve (not of the Henderson-Hasselbalch type). Although the assignment of specific residues to observable phenomena may be naive, it retains some descriptive utility. Site-directed mutagenesis and computational studies often identify key residues, but the experimental data often do not support specific predictions regarding the ionization behavior of individual groups. For example, L212Glu and

L213Asp have been found to be fully or partially charged or neutral, depending on the structure of the RC used in the molecular dynamics simulation (24,25). Most of the electrostatic calculations predict that L212Glu and L213Asp share one proton and that the two residues are never ionized simultaneously independent of the pH (63). On the basis of spectroscopic studies, such as those dealing with the pH dependence of proton binding stoichiometries and the k_{BP} and $k_{AB}(1)$ values (36,37), the pK_a values of L212Glu and L213Asp were estimated to be 9.5 and 4.5, respectively. This means that L212Glu is protonated and L213Asp is ionized at pH 7 (20,21,36,37,64,65). However, because these functional kinetic data are not in full agreement with some steady-state Fourier transform infrared measurements and kinetic infrared (IR) studies, Nabedryk et al. concluded that L212Glu is at least partially ionized and L213Asp is ionized at pH 7 (66). The lack of consensus on the ionization states of the key residues in WT RC makes the revelation of the charge distribution in mutant RCs even more difficult to understand. Any changes in the electric potential due to replacement of key amino acids are hard to predict, even in cases where net positive or negative charges are removed upon mutation. This is because of the complex network of the residues, including 1), strong interaction between the selected amino acid and the neighboring residues, 2), charge rearrangement (solvation and relaxation processes) in the vicinity of the mutation site, and 3), long-range electrostatic or conformational domino effects upon remote mutation.

In contrast to the difficulty of calculating the change in electrostatic potential induced by mutations, indirect measurement of the electrostatic potential is much more reliable. The free energy difference between the Q_A^- Q_B and Q_A Q_B^- states (ΔG^1_{AB}), which corresponds to the electrostatic potential at the Q_B site relative to that of the Q_A site, can be determined from the P^+ Q_B^- $\rightarrow$ PQ_B charge recombination measurements with the assumption of indirect (via the $P^+Q_A^-$ Q_B state) pathway of charge recombination:

$$\Delta G^1_{AB} = -k_B \times T \times \ln\left(\frac{k_{AP}}{k_{BP}} - 1\right). \quad (2)$$

A more negative (positive) potential in the Q_B binding pocket accelerates (decelerates) the P^+ Q_B^- $\rightarrow$ PQ_B charge recombination. Therefore, the charge recombination seems to be a rather simple and useful method of estimating the electrostatic potential at the Q_B site. However, it has some essential drawbacks, and the results derived from charge recombination cannot be directly compared to those obtained from the stigmatellin assay. 1), The charge recombination measurements monitor the difference between the energy levels of the $Q_A^-Q_B$ and $Q_AQ_B^-$ states; thus, it provides the electrostatic potential at the Q_B site relative to that of Q_A. Earlier studies reported small differences in the $Q_A^-Q_B$ energy levels between WT and mutant RCs (36). 2), The charge recombination assay reports on the electrostatic potential in the light-excited RC, whereas the pK_{QB} of stigmatellin in this study monitors the electrostatic potential in the dark-state RC. The ionization states of key residues around the Q_B site are highly different in the dark and light-excited RC, as revealed by computational (25) and experimental studies (66). 3), The rate of the first interquinone electron transfer ($Q_A^-Q_B$ $\leftrightarrow$ $Q_AQ_B^-$) is affected by conformational changes of the protein, which may contribute to the energy level of the $Q_AQ_B^-$ state as well.

Nevertheless, it is highly informative to compare the observed pK_{QB} value of stigmatellin with the free-energy difference of $Q_A^-Q_B$ and $Q_AQ_B^-$ states provided by previous computational and experimental studies (Table 2). The observed pK_{QB} value of stigmatellin in the AA double mutant RC is less by >3.6 pH units than that in the WT RC. The dramatic pK shift corresponds to an at least 210 mV increase in the electrostatic potential. The charge recombination assay and the computational study reported much smaller increases (55 mV and 40 mV, respectively). In the AA+M44Asn$\rightarrow$AA+M44Asp compensatory mutant RC, the shift of pK relative to that in the WT RC is much smaller ($\Delta pK > 0.75$, i.e., 45 mV) and the corresponding increases in electrostatic potential provided by charge recombination and computational studies are 35 mV and 5 mV, respectively. Similarly small increases were found in the compensatory mutant AA+M233Arg$\rightarrow$AA+M233Leu (25 mV (measured) and 30 mV (calculated)). In the other mutants, either the data were not available or the precision of the pK_{QB} determination by the stigmatellin assay was low. The comparison clearly indicates that all three assays report the same sign of changes of the electrostatic potentials induced by mutations, but the magnitudes of the changes are different. The deviations in magnitude can be explained

TABLE 2 pK of stigmatellin bound to the Q_B site of the RC compared with the measured and calculated free-energy difference

	pK_{QB}	ΔG^1_{AB} (meV)	ΔG^1_{AB} (meV)
WT	>11	−60[a]	−80[a]
AA (L212Glu-L213Asp$\rightarrow$Ala-Ala)	7.4	−115[a]	−120[a]
L213Asp$\rightarrow$Ala	7.5	ND	−105[a]
AAY (AA+M249Ala$\rightarrow$AA+M249Tyr)	~7.4	ND	ND
AA+M44Asn$\rightarrow$AA+M44Asp	10.25	−95[a]	−85[a]
AA+M233Arg$\rightarrow$AA+M233Leu	9.5–10.5	−85[a]	−110[a]
AA+L217Arg$\rightarrow$AA+L217Cys	9.5–10.5	−50[b]	ND
L212Glu$\rightarrow$Ala	>10.5	0[a]	−10[a]

The free-energy difference is the difference between the energy levels of $Q_A^-Q_B$ and $Q_AQ_B^-$ states. Values are given for the WT and different mutant RCs. Columns 3 and 4 give the measured and calculated literature values, respectively, at pH 7.0.

[a]Values from Alexov et al. (63).

[b]Value from Valerio-Lepiniec et al. (39).

by the differences in and weaknesses of the assays, discussed above.

To match the consequences from pK_{QB} values of stigmatellin and from flash-induced proton binding stoichiometry data in the different mutant RCs is a far more difficult task because of the complexity of the proton uptake. The proton binding stoichiometry reflects the response of a strongly interacting cluster of protonatable residues and structured water molecules that extends over very large domains of the protein (49). By formation of PQ_A^- or PQ_B^- states, a characteristic band of the proton binding stoichiometry can be observed between pH 9.0 and pH 12.0 (21), which is absent in the mutant RCs of AA, L212Glu→Ala, and AA+M44Asn→AA+M44Asp (33) but is restored in the AAY mutant RC (40). The disappearance and restoration of the high pH band of the proton stoichiometry in different mutants clearly indicates that the high pH band is not the signature of a particular residue. Model calculations showed that the deletion of any group(s) in the strongly anticooperative cluster resulted in the disappearance of the high pH band (41). A similar cooperative mechanism can be assumed to control the observed electric potential in the Q_B binding domain, which is supported also by the results from the suppressor mutants of the AA double mutant. The analogy, however, is not complete, as the L213Asp may play a central role in the cluster. Its replacement by a nonionizable residue in either single or double mutations leads to a significant increase in the potential measured by stigmatellin p*K*. It can be concluded that the electric potential at the Q_B site of the RC is the signature of a particular group, i.e., L213Asp in the cluster.

What kind of mechanism is responsible for the dramatic p*K* drop experienced in the AA mutant RC? The replacement of L213Asp and L212Glu residues by alanine includes a removal of negative charge(s) in the vicinity of the Q_B site. However, in the mutant RC, other residues (e.g., L210Asp), which were neutral in the WT RC, become partially ionized. Although it is highly difficult to predict how the charge distribution changes due to the mutation, it is highly unlikely that only the modified charge distribution is responsible for the dramatic increase (>200 mV) in the electrostatic potential. It is more likely that the mutation induces structural changes that are coupled with the modification of the dielectric feature of the protein. One possible mechanism is that extra water molecules are localized in the Q_B environment or that the arrangement of the water-molecule system is highly different in the AA mutant RC and that the dielectric constant of the medium therefore increases and the electrostatic interactions are screened significantly. Structural investigation of the AA mutant RC revealed that the cavity around the AlaL212 and AlaL213 residues is much larger than in the WT RC and that an extra water molecule is localized exactly in the position of the L213Asp residue of the WT RC. The water molecule forms hydrogen bonds with L223Ser and M44Asn (35). To explain the observed large p*K* drop, in addition to the dominant dielectric effect and the modification of the charge distribution, contributions from other effects, such as the change in the hydrogen-bond network around the Q_B site, cannot be excluded. The crystal structures of the RC revealed chains of ordered water molecules from the cytoplasmic surface to the Q_B site (29). The connected groups of water molecules extend to the common region of L210Asp, M17Asp, and L213Asp (but not L212Glu), which can accommodate one or two water molecule(s). According to Zundel (67), protonated water molecules have a large influence on the H-bonded networks and cause an intense IR continuum band. Indeed, large changes in the IR continuum were observed in single and double mutant RCs where L213Asp was replaced by a neutral residue (22). Bound protonated water molecules located in the vicinity of L213Asp were proposed to be responsible for the specific role of this amino acid. As the electric potential determined by measurement of the p*K* of stigmatellin was also systematically affected by mutations at L213, the same conclusion can be derived: the electric potential changes in the mutant RCs relative to the native RC imply rearrangements of the hydrogen-bonding network in the vicinity of L213. As a consequence of the removal of a negative charge at position of L213, the protonated water molecule(s) will shift the electric potential to more positive values. Confirming the previous IR spectroscopy and structural data, the optical spectroscopy used in this study provided strong evidence for the special role of L213Asp that it can be attributed to its neighboring polarized water molecule(s).

APPENDIX A: DETERMINATION OF THE p*K* OF STIGMATELLIN IN MICELLAR SOLUTION

Formation of micelles from monomers in detergent solution

If n monomers (S) constitute one micelle (M), then the law of mass action for the reaction of $n \times S \overset{K}{\leftrightarrow} M$ is applied:

$$\frac{c_m}{c_1^n} = K, \tag{A1}$$

where K is the equilibrium constant and c_1 and c_m are the concentrations of the free monomers and micelles, respectively, in the solution. The total concentration of all monomers is

$$c_{tot} = c_1 + n \times c_m. \tag{A2}$$

Introducing the critical micelle concentration (CMC) makes it possible to obtain the value of c_{tot}, at which half of the monomers are free and half are assembled into micelles. In other words, $c_1 = n \times c_m = 1/2 \times$ CMC or, substituting into Eq. A1,

$$K = \frac{\frac{CMC}{2n}}{\left(\frac{CMC}{2}\right)^n}. \tag{A3}$$

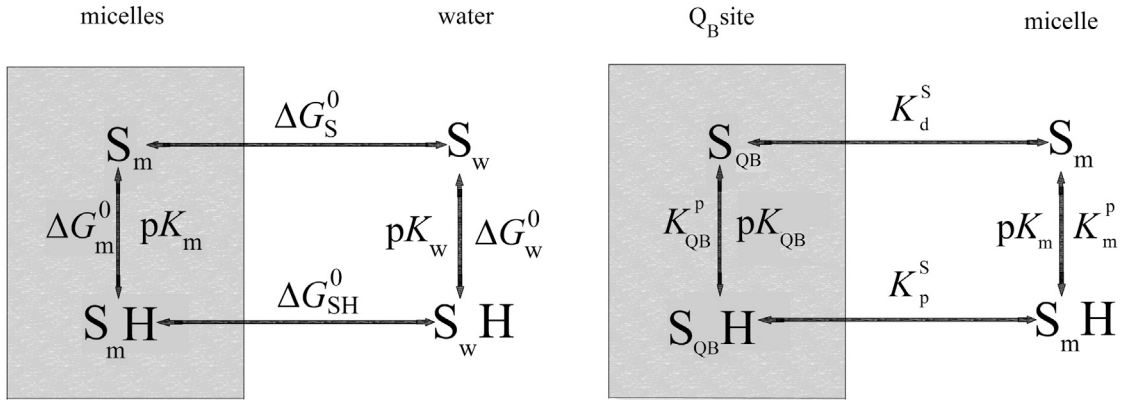

FIGURE A1 (*Left*) Standard free energy changes of the deprotonation (ΔG^0_m, ΔG^0_w) and the transition of the deprotonated (ΔG^0_S) and protonated (ΔG^0_{SH}) forms of stigmatellin between the two phases of the water-micelle system. (*Right*) Equilibrium model of protonation (K^p_{QB}, K^p_m) and dissociation of the stigmatellin (K^S_d, K^S_p) between the Q_B site of the RC and the free micelle.

From Eqs. A1–A3, the micelle concentration as a function of c_{tot} can be expressed implicitly:

$$c_{tot} = \left(\frac{CMC}{2}\right)^{\frac{n-1}{n}} \times (n \times c_m)^{\frac{1}{n}} + n \times c_m. \quad (A4)$$

Whereas at low detergent concentrations ($c_{tot} << CMC$), the first term dominates and $c_m << c_{tot}$ (or c_1), at high detergent concentrations ($c_{tot} >> CMC$), the second term dominates and all detergents form micelles. The CMC is the threshold concentration of the micelle formation.

Stigmatellin in multiphasic solution

The distribution of protonated (SH) and deprotonated (S) forms of stigmatellin in water (w) and in micelles (m) depends on the corresponding free-energy differences (Fig. A1, *left*). In equilibrium, the free energy changes are

$$\Delta G^0_S = G^0_{S,w} - G^0_{S,m} = k_B \times T \times \ln\frac{[S_m]}{[S_w]}, \quad (A5)$$

$$\Delta G^0_{SH} = G^0_{SH,w} - G^0_{SH,m} = k_B \times T \times \ln\frac{[S_mH]}{[S_wH]}, \quad (A6)$$

$$\begin{aligned}\Delta G^0_w &= G^0_{SH,w} - G^0_{S,w} = k_B \times T \times \ln\frac{[S_w]}{[S_wH]} \\ &= k_B \times T \times \ln(10) \times (pH - pK_w),\end{aligned} \quad (A7)$$

$$\begin{aligned}\Delta G^0_m &= G^0_{SH,m} - G^0_{S,m} = k_B \times T \times \ln\frac{[S_m]}{[S_mH]} \\ &= k_B \times T \times \ln(10) \times (pH - pK_m).\end{aligned} \quad (A8)$$

The sum of the free-energy changes along the thermodynamic cycle should be 0:

$$\sum_{i=S,SH,w,m} \Delta G^0_i = 0, \quad (A9)$$

$$\Delta G^0_S - \Delta G^0_{SH} - k_B \times T \times \ln(10) \times (pK_w - pK_m) = 0. \quad (A10)$$

To determine the observed free energy change due to deprotonation of the stigmatellin, we have to relate the total amount of stigmatellin in the protonated state to that in the deprotonated state:

$$\Delta G^{obs}_{SH\to S} = k_B \times T \times n\left(\frac{[S_mH] \times \frac{V_m}{V_w} + [S_wH]}{[S_m] \times \frac{V_m}{V_w} + [S_w]}\right), \quad (A11)$$

where V_m and V_w are the volumes of the membrane and water phases, respectively ($V_m << V_w$). The products of $[S_m] \times V_m/V_w$ and $[S_mH] \times V_m/V_w$ convert the local concentrations to overall concentrations. By introduction of the specific volume (inverse density) of the micelle, $\overline{V_m}$, the ratio of the volumes of the two phases can be expressed as

$$\frac{V_m}{V_w} = \overline{V_m} \times c_m. \quad (A12)$$

The specific volume of a 1.7-nm-radius spherical micelle of of the SDS detergent is $\overline{V_m}$ = 12.3 L/mol (= 0.71 mL/g) (68), which is in the narrow range of 0.70–0.75 mL/g experienced for all proteins (specific volume can be accurately predicted by summing the specific volumes of the component individual amino acids). Based on structural data of the shape and size of the micelles of different detergents, the specific volumes of the micelles can be determined.

By definition, the observed pK (pK^{obs}) is the pH value at which the observed free energy change of deprotonation is equal to 0:

$$\Delta G^{obs}_{SH\to S}(pH = pK^{obs}) = 0. \quad (A13)$$

Substituting Eqs. A5–A7 and A12 into Eq. A11 and the free energy change determining the distribution of the protonated forms of stigmatellin between the two phases, ΔG^0_{SH} from Eq. A10, we get

$$pK^{obs} = \log_{10}\left(\frac{10^{pK_w} + 10^{pK_m} \times \overline{V_m} \times c_m \times \exp\left(\frac{\Delta G^0_S}{k_B T}\right)}{1 + \overline{V_m} \times c_m \times \exp\left(\frac{\Delta G^0_S}{k_B T}\right)}\right). \quad (A14)$$

By inserting c_m from Eq. A4, we can fit the measured data of Fig. 3 using Eq. A14 with two adjustable parameters, pK_m and ΔG_S^0. The parameters obtained from the fit are summarized in Table 1.

APPENDIX B: SCREENING OF THE SURFACE POTENTIAL OF A SPHERICAL MICELLE BY 1-1 ELECTROLYTE

The surface electrostatic potential of a conducting sphere of radius a with $z \times e$ elementary charges in a medium of $\varepsilon = \varepsilon_r \times \varepsilon_0$ absolute permittivity (where ε_r is the relative static permittivity and ε_0 is the dielectric constant of the vacuum) is

$$\psi_0 = \frac{z \times e}{4\pi \times a \times \varepsilon}. \tag{A15}$$

According to the Debye-Hückel theory of dilute solution of strong electrolytes, the ionic clouds diminish the surface potential of the sphere:

$$\psi = \frac{\psi_0}{1 + \kappa \times a}, \tag{A16}$$

where $1/\kappa$ is the Debye length of screening of the solution:

$$\kappa = \sqrt{\frac{2\,e^2 \times N_A}{\varepsilon \times k_B \times T}} \times \sqrt{c}. \tag{A17}$$

Here, N_A is Avogadro's quantity, k_BT is the Boltzmann term, and c is the concentration of the strong 1-1 electrolyte (salt). By substitution of Eq. A17 in Eq. A16, we get

$$\psi = \frac{\psi_0}{1 + a \times \sqrt{\frac{2\,e^2 \times N_A}{\varepsilon \times k_B \times T}} \times c}. \tag{A18}$$

Assuming that the pK of stigmatellin is controlled by the surface potential,

$$pK - pK_\infty = -\frac{\psi}{59\ \text{mV}}, \tag{A19}$$

where pK_∞ denotes the pK of stigmatellin in the absence of electrostatic interaction (at $c \to \infty$) and the term 59 mV is equal to $2.3R \times T/F$ at $T = 298$ K (R is the gas constant, T is the temperature, and F is the Faraday constant). Practically, this pK is measured if stigmatellin is in the hydrophobic phase.

Substituting Eq. A18 into Eq. A19, we obtain

$$\frac{1}{pK - pK_\infty} = -\frac{59\ \text{mV}}{\psi_0} - \frac{59\ \text{mV}}{\psi_0} \times a \times e \times \sqrt{\frac{2\ N_A}{\varepsilon \times k_B \times T}} \times \sqrt{c}. \tag{A20}$$

Inserting the numeric values of $a = 1.7$ nm (radius of the spherical SDS micelle), $e = 1.6 \times 10^{-19}$ C, $k_B = 1.38 \times 10^{-23}$ J $\times$ K^{-1}, $T = 298$ K), $\varepsilon = 7.08 \times 10^{-10}$ A $\times$ s $\times$ V^{-1} $\times$ m^{-1} and $N_A = 6 \times 10^{23}$ mol^{-1}

$$\frac{1}{pK - pK_\infty} = -\frac{59\ \text{mV}}{\psi_0} - \frac{59\ \text{mV}}{\psi_0} \times 5.52 \times \sqrt{c} \times \frac{1}{\sqrt{M}}, \tag{A21}$$

where the concentration, c, should be measured in M = mol L^{-1}. Plotting $1/(pK - pK_\infty)$ as a function of $c^{1/2}$ should yield a straight line. From the slope and intercept, two fitting parameters (pK_∞ and ψ_0) can be derived.

APPENDIX C: ENERGETIC MODEL OF PROTONATION AND BINDING OF STIGMATELLIN TO THE Q_B SITE OF THE RC

The dissociation constant of stigmatellin from the Q_B site at any pH can be expressed with proton binding equilibria of stigmatellin in different phases and with K_d^S (Fig. A1, *right*):

$$\begin{aligned} K^S(\text{pH}) &= \frac{[RC_{free}] \times ([S_mH] + [S_m])}{[SH_{QB}] + [S_{QB}]} \\ &= \frac{[RC_{free}] \times [S_m]}{[S_{QB}]} \times \frac{\left(1 + \frac{[S_mH]}{[S_m]}\right)}{\left(1 + \frac{[S_{QB}H]}{[S_{QB}]}\right)} \\ &= K_d^S \times \frac{1 + 10^{pK_m - pH}}{1 + 10^{pK_{QB} - pH}}. \end{aligned} \tag{A22}$$

Following the conservation of stigmatellin and RC,

$$[S_{total}] = [S_mH] + [S_m] + [S_{QB}] + [S_{QB}H], \tag{A23}$$

$$[RC_{total}] = [RC_{free}] + [S_{QB}] + [S_{QB}H]. \tag{A24}$$

Inserting Eqs. A23 and A24 into Eq. A22 gives

$$K^S(\text{pH}) = \frac{([RC_{total}] - ([S_{QB}] + [S_{QB}H])) \times ([S_{total}] - ([S_{QB}] + [S_{QB}H]))}{[S_{QB}H] + [S_{QB}]}. \tag{A25}$$

Only that solution of Eq. A25 is taken, which has physical meaning

$$[S_{QB}H] + [S_{QB}] = \frac{[RC_{total}] + [S_{total}] + K^S(\text{pH}) - \sqrt{([RC_{total}] + [S_{total}] + K^S(\text{pH}))^2 - 4[RC_{total}] \times [S_{total}]}}{2}. \tag{A26}$$

After $[S_{QB}]$ is expressed with $[S_{QB}H]$ using the Henderson-Hasselbalch equation and Eq. A22 is inserted into Eq. A26, $[S_{QB}H]$ is expressed by the known ($[RC_{total}]$, $[S_{total}]$, pK_m, and pH) and unknown fitting parameters (pK_{QB} and K_d^S):

$$[S_{QB}H] = \frac{[RC_{total}] + [S_{total}] + K_d^S \times \frac{1+10^{pK_m-pH}}{1+10^{pK_{QB}-pH}} - \sqrt{\left([RC_{total}] + [S_{total}] + K_d^S \times \frac{1+10^{pK_m-pH}}{1+10^{pK_{QB}-pH}}\right)^2 - 4[RC_{total}] \times [S_{total}]}}{2\ (1+10^{pH-pK_{QB}})}. \quad \text{(A27)}$$

Similar equations can be written also for $[S_{QB}]$, $[S_mH]$, and $[S_m]$.

At a given pH, the absorption of the stigmatellin is a weighted sum of the extinction coefficients of the protonated and deprotonated forms of stigmatellin, where the weights are the concentrations of the different forms:

$$A_{obs} = \varepsilon_p \times l \times \left([S_{QB}H] + [S_mH]\right) + \varepsilon_d \times l \times \left([S_{QB}] + [S_m]\right). \quad \text{(A28)}$$

By introducing the spectroscopic ratio and taking into account that $\varepsilon_p(287) = \varepsilon_d(287)$ and $\varepsilon_p(300) = \varepsilon_d(300)$

$$\frac{A_{obs}(278) - A_{obs}(300)}{A_{obs}(287) - A_{obs}(300)} = \frac{\varepsilon_p(278) - \varepsilon_p(300)}{\varepsilon_p(287) - \varepsilon_p(300)} \times \frac{\left([S_{QB}H] + [S_mH]\right)}{[S_{total}]} + \frac{\varepsilon_d(278) - \varepsilon_d(300)}{\varepsilon_d(287) - \varepsilon_d(300)} \times \frac{\left([S_{QB}] + [S_m]\right)}{[S_{total}]}. \quad \text{(A29)}$$

Inserting Eq. A27 and the corresponding equations for $[S_{QB}]$, $[S_mH]$, and $[S_m]$ into Eq. A29, the spectroscopic ratio as a function of the stigmatellin concentration at a given pH can be fitted by two parameters, pK_{QB} and K_d^S.

In the presence of a large quinone pool, the competitive binding of quinone and stigmatellin to the Q_B site should be described. Equation A24 is extended with $[Q_{QB}]$ and the quinone conservation and quinone binding equilibrium are defined as

$$[RC_{total}] = [RC_{free}] + [S_{QB}] + [S_{QB}H] + [Q_{QB}], \quad \text{(A30)}$$

$$[Q_{total}] = [Q_{free}] + [Q_{QB}], \quad \text{(A31)}$$

$$K_Q = \frac{[RC_{free}] \times [Q_{free}]}{[Q_{QB}]}. \quad \text{(A32)}$$

Equations A30–A32 in combination with Eqs. A22 and A23 give a nonlinear system of equations with five unknown quantities ($[RC_{free}]$, $[Q_{free}]$, $[Q_{QB}]$, $[S_{QB}]$, and $[S_{QB}H]$) and three fitting parameters, K_Q, K_d^S, and pK_{QB}. By solving the system of equations using the $[S_{QB}]$, $[S_{QB}H]$, $[S_m]$, and $[S_mH]$ values the spectroscopic ratio can be calculated with Eq. A29. The fitting parameters of K_d^S and pK_{QB} have already been determined from Fig. 7, *left*, where the quinone content was negligible. The fitting parameter of K_Q can be acquired from Fig. 7, *right*.

SUPPORTING MATERIAL

One figure is available at http://www.biophysj.org/biophysj/supplemental/S0006-3495(14)04676-1.

ACKNOWLEDGMENTS

We are indebted to Drs. László Kálmán (Concordia University, Montreal, Canada) and Eiji Takahashi (University of Illinois, Urbana, IL) for their work in the early phase of this project. This work is dedicated to the memory of Colin A. Wraight, who passed away on July 10, 2014.

This study has been supported by Társadalmi Megújulás Operatív Program grants TÁMOP 4.2.2.A-11/1KONV-2012-0060, TÁMOP 4.2.2.B, and COST European Cooperation in Sciences and Technology grant CM1306. L.G. is grateful to the FOM (No. 126) for financial support.

REFERENCES

1. Lancaster, C. R. D. 2003. The role of electrostatics in proton-conducting membrane protein complexes. *FEBS Lett.* 545:52–60.
2. Starke-Peterkovic, T., N. Turner, …, R. J. Clarke. 2006. Cholesterol effect on the dipole potential of lipid membranes. *Biophys. J.* 90:4060–4070.
3. Pilotelle-Bunner, A., P. Beaunier, …, P. Sebban. 2009. The local electric field within phospholipid membranes modulates the charge transfer reactions in reaction centres. *Biochim. Biophys. Acta.* 1787:1039–1049.
4. Starke-Peterkovic, T., N. Turner, …, R. J. Clarke. 2005. Electric field strength of membrane lipids from vertebrate species: membrane lipid composition and Na^+-K^+-ATPase molecular activity. *Am. J. Physiol. Regul. Integr. Comp. Physiol.* 288:R663–R670.
5. Rokitskaya, T. I., E. A. Kotova, and Y. N. Antonenko. 2002. Membrane dipole potential modulates proton conductance through gramicidin channel: movement of negative ionic defects inside the channel. *Biophys. J.* 82:865–873.
6. Buzón, V., and J. Cladera. 2006. Effect of cholesterol on the interaction of the HIV GP41 fusion peptide with model membranes. Importance of the membrane dipole potential. *Biochemistry.* 45:15768–15775.
7. Wraight, C. A. 2004. Proton and electron transfer in the acceptor quinone complex of photosynthetic reaction centers from *Rhodobacter sphaeroides*. *Front. Biosci.* 9:309–337.
8. Onidas, D., G. Sipka, …, P. Maróti. 2013. Mutational control of bioenergetics of bacterial reaction center probed by delayed fluorescence. *Biochim. Biophys. Acta.* 1827:1191–1199.
9. Tyner, K. M., R. Kopelman, and M. A. Philbert. 2007. "Nanosized voltmeter" enables cellular-wide electric field mapping. *Biophys. J.* 93:1163–1174.

10. Surek, J. T., and D. D. Thomas. 2008. A paramagnetic molecular voltmeter. *J. Magn. Reson.* 190:7–25.
11. Cohen, B. E., T. B. McAnaney, …, L. Y. Jan. 2002. Probing protein electrostatics with a synthetic fluorescent amino acid. *Science.* 296:1700–1703.
12. Lehle, H., J. M. Kriegl, …, G. U. Nienhaus. 2005. Probing electric fields in protein cavities by using the vibrational stark effect of carbon monoxide. *Biophys. J.* 88:1978–1990.
13. Philippsen, A., W. Im, …, D. J. Müller. 2002. Imaging the electrostatic potential of transmembrane channels: atomic probe microscopy of OmpF porin. *Biophys. J.* 82:1667–1676.
14. Junge, W., and H. T. Witt. 1968. On the ion transport system of photosynthesis—investigations on a molecular level. *Z. Naturforsch. B.* 23:244–254.
15. Asztalos, E., G. Sipka, …, P. Maróti. 2012. The reaction center is the sensitive target of the mercury(II) ion in intact cells of photosynthetic bacteria. *Photosynth. Res.* 112:129–140.
16. Ephard, H., and P. Fromherz. 1989. Fluorescence and photoisomerization of an amphiphilic aminostilbazolium dye as controlled by the sensitivity of radiationless deactivation to polarity and viscosity. *J. Phys. Chem.* 93:7717–7725.
17. Okamura, M. Y., M. L. Paddock, …, G. Feher. 2000. Proton and electron transfer in bacterial reaction centers. *Biochim. Biophys. Acta.* 1458:148–163.
18. Wraight, C. A., and M. R. Gunner. 2009. The acceptor quinones of purple photosynthetic bacteria: structure and spectroscopy. *In* Advances in Photosynthesis and Respiration: The Purple Phototrophic Bacteria. C. N. Hunter, F. Daldal, M. C. Thurnauer, and J. T. Beatty, editors. Springer, Dordrecht, The Netherlands, pp. 379–405.
19. Graige, M. S., M. L. Paddock, …, M. Y. Okamura. 1996. Mechanism of proton-coupled electron transfer for quinone (Q_B) reduction in reaction centers of *Rb. Sphaeroides*. *J. Am. Chem. Soc.* 118:9005–9016.
20. Sebban, P., P. Maróti, and D. K. Hanson. 1995. Electron and proton transfer to the quinones in bacterial photosynthetic reaction centers: insight from combined approaches of molecular genetics and biophysics. *Biochimie.* 77:677–694.
21. Maróti, P., and C. A. Wraight. 1988. Flash-induced H^+ binding by bacterial photosynthetic reaction centers: Influences of the redox states of the acceptor quinones and primary donors. *Biochim. Biophys. Acta.* 934:329–347.
22. Nabedryk, E., and J. Breton. 2008. Coupling of electron transfer to proton uptake at the Q_B site of the bacterial reaction center: a perspective from FTIR difference spectroscopy. *Biochim. Biophys. Acta.* 1777:1229–1248.
23. Taguchi, A. T., A. J. Mattis, …, C. A. Wraight. 2013. Tuning cofactor redox potentials: the 2-methoxy dihedral angle generates a redox potential difference of >160 mV between the primary (Q_A) and secondary (Q_B) quinones of the bacterial photosynthetic reaction center. *Biochemistry.* 52:7164–7166.
24. Rabenstein, B., G. M. Ullmann, and E. W. Knapp. 2000. Electron transfer between the quinones in the photosynthetic reaction center and its coupling to conformational changes. *Biochemistry.* 39:10487–10496.
25. Zhu, Z., and M. R. Gunner. 2005. Energetics of quinone-dependent electron and proton transfers in *Rhodobacter sphaeroides* photosynthetic reaction centers. *Biochemistry.* 44:82–96.
26. Remy, A., and K. Gerwert. 2003. Coupling of light-induced electron transfer to proton uptake in photosynthesis. *Nat. Struct. Biol.* 10:637–644.
27. Breton, J. 2004. Absence of large-scale displacement of quinone Q_B in bacterial photosynthetic reaction centers. *Biochemistry.* 43:3318–3326.
28. Maróti, P., and C. A. Wraight. 1997. Kinetics of H^+ ion binding by the $P^+Q_A^-$ state of bacterial photosynthetic reaction centers: rate limitation within the protein. *Biophys. J.* 73:367–381.
29. Fritzsch, G., J. Koepke, …, L. Baciou. 2002. Charge separation induces conformational changes in the photosynthetic reaction centre of purple bacteria. *Acta Crystallogr. D Biol. Crystallogr.* 58:1660–1663.
30. Hanson, D. K., D. M. Tiede, …, M. Schiffer. 1993. Site-specific and compensatory mutations imply unexpected pathways for proton delivery to the QB binding site of the photosynthetic reaction center. *Proc. Natl. Acad. Sci. USA.* 90:8929–8933.
31. Maróti, P., D. K. Hanson, …, P. Sebban. 1994. Proton conduction within the reaction centers of *Rhodobacter capsulatus*: the electrostatic role of the protein. *Proc. Natl. Acad. Sci. USA.* 91:5617–5621.
32. Hanson, D. K., L. Baciou, …, P. Sebban. 1992. In bacterial reaction centers protons can diffuse to the secondary quinone by alternative pathways. *Biochim. Biophys. Acta.* 1102:260–265.
33. Miksovska, J., P. Maróti, …, P. Sebban. 1996. Distant electrostatic interactions modulate the free energy level of Q_A^- in the photosynthetic reaction center. *Biochemistry.* 35:15411–15417.
34. Miksovska, J., L. Kálmán, …, D. K. Hanson. 1997. In bacterial reaction centers rapid delivery of the second proton to Q_B can be achieved in the absence of L212Glu. *Biochemistry.* 36:12216–12226.
35. Pokkuluri, P. R., P. D. Laible, …, M. Schiffer. 2002. The structure of a mutant photosynthetic reaction center shows unexpected changes in main chain orientations and quinone position. *Biochemistry.* 41: 5998–6007.
36. Maróti, P., D. K. Hanson, …, P. Sebban. 1995. Long-range electrostatic interaction in the bacterial photosynthetic reaction centre. *Nat. Struct. Biol.* 2:1057–1059.
37. Takahashi, E., and C. A. Wraight. 1992. Proton and electron transfer in the acceptor quinone complex of *Rhodobacter sphaeroides* reaction centers: characterization of site-directed mutants of the two ionizable residues, Glu^{L212} and Asp^{L213}, in the Q_B binding site. *Biochemistry.* 31:855–866.
38. Paddock, M. L., S. H. Rongey, …, M. Y. Okamura. 1994. Pathway of proton transfer in bacterial reaction centers: role of aspartate-L213 in proton transfers associated with reduction of quinoneto dihydroquinone. *Biochemistry.* 33:734–745.
39. Valerio-Lepiniec, M., J.-D. Delcroix, …, P. Sebban. 1997. A native electrostatic environment near Q_B is not sufficient to ensure rapid proton delivery in photosynthetic reaction centers. *FEBS Lett.* 407: 159–163.
40. Tandori, J., L. Baciou, …, P. Sebban. 2001. Revealing the involvement of extended hydrogen bond networks in the cooperative function between distant sites in bacterial reaction centers. *J. Biol. Chem.* 276:45513–45515.
41. Cheap, H., J. Tandori, …, P. Sebban. 2007. Evidence for delocalized anticooperative flash induced proton binding as revealed by mutants at the M266His iron ligand in bacterial reaction centers. *Biochemistry.* 46:4510–4521.
42. Giangiacomo, K. M., D. E. Robertson, …, P. L. Dutton. 1987. Stigmatellin and other electron transfer inhibitors as probes for the Q_B binding site in the reaction center of photosynthetic bacteria. *In* Progress in Photosynthesis Research. J. Biggins, editor. Martinus Nijhoff, Dordrecht, The Netherlands, pp. 409–412.
43. Oettmeier, W., D. Godde, …, G. Höfle. 1985. Stigmatellin. A dual type inhibitor of photosynthetic electron transport. *Biochim. Biophys. Acta.* 807:216–219.
44. Thierbach, G., B. Kunze, …, G. Höfle. 1984. The mode of action of stigmatellin, a new inhibitor of the cytochrome bc_1 segment of the respiratory chain. *Biochim. Biophys. Acta.* 765:227–235.
45. von Jagow, G., and T. Ohnishi. 1985. The chromone inhibitor stigmatellin—binding to the ubiquinol oxidation center at the C-side of the mitochondrial membrane. *FEBS Lett.* 185:311–315.
46. Swainsbury, D. J. K., V. M. Friebe, …, M. R. Jones. 2014. Evaluation of a biohybrid photoelectrochemical cell employing the purple bacterial reaction centre as a biosensor for herbicides. *Biosens. Bioelectron.* 58:172–178.
47. Ginet, N., and J. Lavergne. 2001. Equilibrium and kinetic parameters for the binding of inhibitors to the Q_B pocket in bacterial chromatophores: dependence on the state of Q_A. *Biochemistry.* 40:1812–1823.
48. Lancaster, C. R. D., and H. Michel. 1997. The coupling of light-induced electron transfer and proton uptake as derived from crystal

structures of reaction centres from *Rhodopseudomonas viridis* modified at the binding site of the secondary quinone, Q_B. *Structure.* 5:1339–1359.

49. Lancaster, C. R. D., C. Hunte, …, R. Ditchfield. 2007. A comparison of stigmatellin conformations, free and bound to the photosynthetic reaction center and the cytochrome bc_1 complex. *J. Mol. Biol.* 368: 197–208.
50. Graige, M. S., M. L. Paddock, G. Feher, and M. Y. Okamura. 1996. Using stigmatellin to probe the electrostatic environment of the QB site in bacterial RCs. *Biophys. J.* 70: Supplement, Abstract, A11.
51. Gerencsér, L., L. Rinyu, …, P. Maróti. 2004. Competitive binding of quinone and antibiotic stigmatellin to reaction centers of photosynthetic bacteria. *Acta Biol. Szeged.* 48:25–33.
52. Maróti, P., and C. A. Wraight. 1988. Flash-induced H^+ binding by bacterial photosynthetic reaction centers: comparison of spectrometric and conductometric methods. *Biochim. Biophys. Acta.* 934:314–328.
53. Baciou, L., and H. Michel. 1995. Interruption of the water chain in the reaction center from *Rhodobacter sphaeroides* reduces the rates of the proton uptake and of the second electron transfer to Q_B. *Biochemistry.* 34:7967–7972.
54. Dutkiewicz, E., and A. Jakubowska. 2002. Effect of electrolytes on the physicochemical. behaviour of sodium dodecyl sulphate micelles. *Colloid Polym. Sci.* 280:1009–1014.
55. Gast, P., P. W. Hemelrijk, …, A. J. Hoff. 1996. The association of different detergents with the photosynthetic reaction center protein of *Rhodobacter sphaeroides* R26 and the effects on its photochemistry. *Eur. J. Biochem.* 239:805–809.
56. Hanson, D. K., S. L. Nance, and M. Schiffer. 1992. Second-site mutation at M43 (Asn→Asp) compensates for the loss of two acidic residues in the Q_B site of the reaction center. *Photosynth. Res.* 32:147–153.
57. Sebban, P., P. Maróti, …, D. K. Hanson. 1995. Electrostatic dominoes: long distance propagation of mutational effects in photosynthetic reaction centers of *Rhodobacter capsulatus*. *Biochemistry.* 34:8390–8397.
58. Graige, M. S., M. L. Paddock, …, M. Y. Okamura. 1999. Observation of the protonated semiquinone intermediate in isolated reaction centers from *Rhodobacter sphaeroides*: implications for the mechanism of electron and proton transfer in proteins. *Biochemistry.* 38:11465–11473.
59. Stowell, M. H. B., T. M. McPhillips, …, G. Feher. 1997. Light-induced structural changes in photosynthetic reaction center: implications for mechanism of electron-proton transfer. *Science.* 276:812–816.
60. Xu, Q., L. Baciou, …, M. R. Gunner. 2002. Exploring the energy landscape for Q_A^- to Q_B electron transfer in bacterial photosynthetic reaction centers: effect of substrate position and tail length on the conformational gating step. *Biochemistry.* 41:10021–10025.
61. Gunner, M. R., M. A. Saleh, …, M. Wise. 2000. Backbone dipoles generate positive potentials in all proteins: origins and implications of the effect. *Biophys. J.* 78:1126–1144.
62. Lancaster, C. R. D., H. Michel, …, M. R. Gunner. 1996. Calculated coupling of electron and proton transfer in the photosynthetic reaction center of *Rhodopseudomonas viridis*. *Biophys. J.* 70:2469–2492.
63. Alexov, E., J. Miksovska, …, M. R. Gunner. 2000. Modeling the effects of mutations on the free energy of the first electron transfer from Q_A^- to Q_B in photosynthetic reaction centers. *Biochemistry.* 39:5940–5952.
64. Brzezinski, P., M. L. Paddock, …, G. Feher. 1997. Light-induced electrogenic events associated with proton uptake upon forming Q_B^- in bacterial wild-type and mutant reaction centers. *Biochim. Biophys. Acta.* 1321:149–156.
65. Ishikita, H., G. Morra, and E. W. Knapp. 2003. Redox potential of quinones in photosynthetic reaction centers from *Rhodobacter sphaeroides*: dependence on protonation of Glu-L212 and Asp-L213. *Biochemistry.* 42:3882–3892.
66. Nabedryk, E., M. L. Paddock, …, J. Breton. 2007. Monitoring the pH dependence of IR carboxilic acid signals upon Q_B^- formation in the Glu-L212→Asp/Asp-L213→Glu swap mutant reaction center from *Rhodobacter sphaeroides*. *Biochemistry.* 46:1176–1182.
67. Zundel, G. 2000. Hydrogen bonds with large proton polarizability and proton transfer processes in electrochemistry and biology. *In* Advances in Chemical Physics, *Vol. 111*. I. Prigogine, and S. A. Rice, editors. John Wiley & Sons, Hoboken, NJ, pp. 1–217.
68. Israelachvili, J. N. 1991. Intermolecular and Surface Forces, 2nd ed. Academic Press, London.